Climatic Change (2020) 162:583–601
https://doi.org/10.1007/s10584-020-02833-z

Assessing uncertainties in the regional projections of precipitation in CORDEX-AFRICA

Adeline Bichet[1] · Arona Diedhiou[1,2] · Benoit Hingray[1] · Guillaume Evin[3] · N'Datchoh Evelyne Touré[2] · Klutse Nana Ama Browne[4] · Kouakou Kouadio[2]

Received: 14 October 2019 / Accepted: 12 August 2020 / Published online: 11 September 2020

Abstract

Over the past decades, large variations of precipitation were observed in Africa, which often led to dramatic consequences for local society and economy. To avoid such disasters in the future, it is crucial to better anticipate the expected changes, especially in the current context of climate change and population growth. To this date, however, projections of precipitation over Africa are still associated with very large uncertainties. To better understand how this uncertainty can be reduced, this study uses an advanced Bayesian analysis of variance (ANOVA) method to characterize, for the first time in the regional climate projections of CORDEX-AFRICA, the different sources of uncertainty associated with the projections of precipitation over Africa.

By 2090, the ensemble mean precipitation is projected to increase over the Horn of Africa from September to May and over the eastern Sahel and Guinea Coast from June to November. It is projected to decrease over the northern coast and southern Africa all year long, over western Sahel from March to August, and over the Sahel and Guinea Coast from March to May. Most of these projections however are not robust, i.e., the magnitude of change is smaller than the associated uncertainty. Over time, the relative contribution of internal variability (excluding interannual variability) to total uncertainty is moderate and quickly falls below 10%. By 2090, it is found that over the Horn of Africa, northern coast, southern Africa, and Sahel, most of the uncertainty results from a large dispersion across the driving Global Climate Models (in particular MIROC, CSIRO, CCCma, and IPSL), whereas over the tropics and parts of eastern Africa, most of the uncertainty results from a large dispersion across Regional Climate Models (in particular CLMcom).

Keywords CORDEX-AFRICA · Precipitation · Bayesian ANOVA · Model uncertainty · Internal variability

Electronic supplementary material The online version of this article (https://doi.org/10.1007/s10584-020-02833-z) contains supplementary material, which is available to authorized users.

✉ Adeline Bichet
adeline.bichet@univ–grenoble–alpes.fr

Extended author information available on the last page of the article

1 Introduction

Global warming is expected to have substantial consequences on precipitation and its variability, especially extreme events, potentially leading to more frequent and severe droughts and flood episodes in both, the tropics and the subtropical regions (Zwiers et al. 2013; Giorgi et al. 2014). Precipitation is the main driver of the variability of water resources, and Africa is particularly vulnerable to its variations, especially in the rural areas where agriculture is the most prominent activity for securing income and overcoming poverty (Boko et al. 2007). Africa is also exposed to high water stress and scarcity (Schewe et al. 2014), along with recurrent droughts and floods (Douglas et al. 2008; Dai 2013). These conditions, expected to be exacerbated in the future, constitute significant threats to water resources, agricultural activities, and ecosystem services (Lobell et al. 2011; Anyamba et al. 2014).

For the twenty-first century, however, the 5th Assessment Report (AR5) of the Intergovernmental Panel on Climate Change (IPCC) showed that projections of mean precipitation over Africa are highly uncertain, the expected changes do not exceed the baseline variability in more than 66% of the Coupled Model Intercomparison Project (CMIP5) models (Niang et al. 2014) over most of the continent. The exceptions include a "likely" (exceed the baseline variability in more than 66% of the CMIP5 models) decrease of annual mean precipitation over the northern (Mediterranean) coast of Africa and southern Africa, and a "very likely" (exceed the baseline variability in more than 90% of the CMIP5 models) increase of annual mean precipitation over central and most of eastern Africa. Over western Africa and parts of eastern Africa (including Ethiopian Highlands, Great Lakes), however, no clear trend is detected and the confidence in projections is extremely low (Niang et al. 2014). These uncertainties and large ensemble spread in the projections of precipitation by CMIP5 Global Climate Models (GCMs) have been reported by Diedhiou et al. (2018) when investigating changes in climate extremes over West and Central Africa at 1.5 °C and 2 °C global warming. According to previous studies (Rowell 2012; Orlowsky and Seneviratne 2012), the large uncertainties associated with global climate projections of precipitation over Africa are partly due to the strong interannual variability of precipitation (generally over arid regions) and to strong disagreements across GCMs; amplitude and sign of change, generally over the tropics). Recent studies have shown that these disagreements can be partially attributed to the inability of GCMs to resolve convective rainfall (Christensen et al. 2007; Fontaine et al. 2011; Roehrig et al. 2013). Uncertainties in land surface processes and interactions with atmosphere contribute also to a large spread of GCM projections in regions where the vegetation and soil moisture are strongly interlinked with precipitation and temperature (Koster et al. 2004; He et al. 2017; Donat et al. 2018).

The release of multiple ensemble downscaled projections such as those produced through the Coordinated Regional Downscaling Experiment for Africa (CORDEX-AFRICA; Giorgi et al. 2009; Jones et al. 2011; Hewitson et al. 2012; Nikulin et al. 2012) is expected to improve the results, as the high resolution (~ 50 km) of Regional Climate Models (RCMs) used in these projections allows a better representation of topographical details and local processes such as convection. Over eastern Africa for instance, RCMs project wetter conditions over most of the region (including the Horn of Africa), as seen in the GCMs, but in addition they also project dryer conditions over highly convective areas such as the Ethiopian Highlands in March–April–May (MAM; Dosio et al. 2019) and the Great Lakes in June–July–August (JJA; Niang et al. 2014), thus suggesting an improvement from global climate projections and highlighting the importance of resolving both, regional-scale atmospheric processes and local effects such

as land surface. Over central and western Africa however, large uncertainties remain in regional climate projections (Dosio et al. 2019). Even though the multi-model mean of CORDEX-AFRICA shows a significant increase (decrease) in mean precipitation over the Guinea Coast (the Sahel, especially over the western Sahel; Sylla et al. 2016; Todzo et al. 2020), individual RCMs strongly disagree on the projected sign of change. According to Klutse et al. (2015), most of the substantial differences in daily precipitation characteristics simulated by the RCMs of CORDEX-AFRICA are driven by their different convective schemes.

To better understand the different sources of uncertainty associated with the regional projections of precipitation over Africa, our study uses an advanced Bayesian analysis of variance (ANOVA) method that allows quantifying, for the first time in the regional climate projections of CORDEX-AFRICA, (1) an estimate of the mean projected precipitation "forced response", i.e., the mean projected response of the CORDEX-AFRICA ensemble to external radiative forcing for the considered emissions scenario; (2) an estimate of the total uncertainty associated to the projections of this ensemble; (3) the relative contribution of each source of uncertainty; and (4) the individual contribution of each model to model uncertainty. The different sources of uncertainty targeted in this study are as follows: internal unforced variability (natural variability that results from the chaotic and unpredictable nonlinear nature of the climate system) and model uncertainty due to GCMs and RCMs separately, i.e., climate response uncertainty that results from structural differences between models. Model uncertainty (RCMs and GCMs) arises from different model configurations such as the number of vertical levels, the numerical scheme used to solve the equations, and the implementation of surface characteristics (land use information), as well as different parametrization schemes used to represent sub-grid processes such as convection, cloud cover properties, and aerosol interactions. Note that the CORDEX framework implies that all the RCMs are operated on the same spatial scales and forced with identical climate forcings for a given emission scenario. They are forced with different boundary conditions (i.e., large-scale meteorological fields such as air temperature, humidity, zonal and meridional wind, geopotential height, surface air pressure, and sea surface temperatures) from the different GCMs respectively.

Thus, our study allows us to identify to which extent the uncertainty associated to the regional projections of precipitation from CORDEX-AFRICA results from internal variability and is thereby irreducible, and to which extent it results from model uncertainty and is thereby reducible through the improvement of RCMs or GCMs. Section 2 describes the methodology. Section 3 presents the results of our analyses for 2090 (Sections 3.1 and 3.2) and throughout the twenty-first century (Section 3.3). Section 4 discusses the results for each region, and Section 5 concludes.

2 Methodology and data

2.1 Datasets

We use an ensemble of 14 regional climate simulations from the most up-to-date ensemble of high-resolution RCM projections produced in the recent years for Africa: CORDEX-AFRICA (Giorgi et al. 2009; Jones et al. 2011; Hewitson et al. 2012; Nikulin et al. 2012). In this ensemble, four RCMs are used to downscale nine GCM experiments obtained in CMIP5 under the RCP8.5 climate scenario (Table 1). The simulations span the period 1976–2100 over entire

Table 1 Summary of 14 simulations taken from the CORDEX-AFRICA data. In this ensemble, four RCMs are used to downscale nine GCM experiments obtained in CMIP5. Each experiment comprises one historical and one scenario (RCP8.5) run, spanning the periods 1976–2005 and 2006–2100, respectively. The horizontal resolution of all simulations is 0.44° in both latitude and longitude

RCM\GCM	DMI-HIRHAM5 (DMI)	CLMcom-CCLM4-8-17 (CLMcom)	KNMI-RACMO22T (KNMI)	SMHI-RCA4 (SMHI)
ICHEC-EC-EARTH (ICHEC)	x	x	x	x
CNRM-CERFACS-CNRM-CM5 (CNRM)		x		x
MPI-M-MPI-ESM-LR (MPI)		x		x
NCC-NorESM1-M (NCC)				x
NOAA-GFDL-GFDL-ESM2M (NOAA)				x
IPSL-IPSL-CM5A-MR (IPSL)				x
MIROC-MIROC5 (MIROC)				x
CSIRO-QCCCE-CSIRO-Mk3-6-0 (CSIRO)				x
CCCma-CanESM2 (CCCma)				x

Africa (24.64° W–60.28° E; 45.76° S–42.24° N) with a spatial resolution of 0.44° (~ 50 km) in latitude and longitude. Historical simulations cover the period 1976–2005 while projections following the RCP8.5 scenarios cover the period 2006–2100, the two sets of simulations being tailored to be combined with each other. For each simulation and each grid cell, the daily time series of precipitation are retrieved.

As an important prerequisite for this work, we evaluate the simulated mean precipitation over the period 1981–2014, by comparison with the observed mean precipitation taken from the Climate Hazards Group InfraRed Precipitation with Station (CHIRPS) dataset (Funk et al. 2015). In all four seasons, we find that the ensemble mean (Supplementary Fig. 1a) satisfactorily captures the observed (Supplementary Fig. 1b) spatial distribution averaged over 1981–2014, showing a band of precipitation located over (a) 0–15° N in June–July–August (JJA; up to 8 mm/day over the Sahel and the Guinea Coast), (b) 12° S–12° N in September–October–November (SON; up to 8 mm/day over the Guinea Coast), (c) 15° S–0° in December–January–February (DJF; up to 8 mm/day over Mozambique, Malawi, and Zambia), and (d) 12° S–5° N in March–April–May (MAM; up to 8 mm/day over the Guinea Coast). Elsewhere, precipitation is generally lower than 1 mm/day in JJA and DJF, and lower than 3 mm/day in SON and MAM. Thus, both datasets overall show dry conditions (below 3 mm/day all year long) over the mid-latitudes (15° N–30° N and 15° S–30° S) and wetter conditions (between 2 and 8 mm/day depending on the season) over the tropics (15° S–15° N). In all seasons, however, the ensemble mean slightly underestimates (overestimates) the observations over the tropics (the Sahel and southern Africa; Supplementary Fig. 1c). In addition, we also evaluate the simulated temporal variability (daily and annual) of precipitation over the period 1981–2014, by comparison with the observed variability, and as averaged over the nine regions depicted in Supplementary Fig. 2. As in Bichet et al. (2019), these nine regions are adapted from the IPCC SREX regions (e.g., Giorgi and Francisco 2000; Seneviratne et al. 2012; Christensen et al. 2013), accounting for additional sub-regional climate differences. For instance, we split the IPCC SREX region "East Africa" into two different sub-regions in order to separate the Great Lakes area (Region 6, East Africa) from the mountainous areas of the Ethiopian Highlands (Region 7, Horn of Africa). Similarly, we split the IPCC SREX region

"West Africa" into three different sub-regions to separate the dry Sahel (Region 3, West Sahel and Region 4, East Sahel) from the wet Guinea Coast (Region 5, Guinea Coast). We find that in all the nine regions, the observed variability (daily and annual) is encompassed within the range of model dispersion (Supplementary Fig. 3). In addition, Todzo et al. (2020) showed that the statistical distribution of daily mean and annual mean precipitation simulated in three West African cities (Dakar, Ouagadougou, and Accra) over 1981–2014 by 19 individual members of the CORDEX-AFRICA ensemble fit rather well the observation (CHIRPS dataset and the rain gauge stations). We conclude that the overall good agreement between the simulated and observed precipitation encourages the use of the CORDEX-AFRICA ensemble for investigating the sources of uncertainty associated with the regional projections of precipitation in Africa.

2.2 Methodology

To partition and quantify the different sources of uncertainty (i.e., internal variability, GCM uncertainty, and RCM uncertainty) associated with the regional climate projections from CORDEX-AFRICA, we use QUALYPSO (Evin et al. 2019), an advanced Bayesian analysis of variance (ANOVA) method based on data augmentation techniques and on the quasi-ergodicity assumption of climate outputs (Hingray and Saïd 2014; Hingray et al. 2019). More specifically, in QUALYPSO, missing GCM/RCM combinations are part of the inference process. As shown in Evin et al. (2019), missing RCM/GCM combinations usually lead to biases when direct ANOVA estimates are produced. Conversely to typical ANOVA approaches used for such analysis, QUALYPSO allows for a robust partition and unbiased estimation of all uncertainty components in multi-member multi-model ensembles of regional climate projections, even in the case of single run ensembles (i.e., when only one experiment is available for some or all the GCM/RCM combinations; which is the case here as only one experiment is available for each GCM/RCM combination) and even when ensembles are incomplete (i.e., when not all GCM/RCM combinations are available, which is also the case here as only 14 GCM/RCM combinations are available out of the 36 (= 9 × 4) possible GCM/RCM combinations; Table 1).

In the following, we use QUALYPSO to quantify uncertainty sources of the 20-year running mean (annual and seasonal mean aggregated from the daily time series) projections (1976–2100) of precipitation for each grid cell of the African continent and has averaged over the nine regions depicted in Supplementary Fig. 2. More specifically, we estimate (1) the mean projected precipitation "forced response", i.e., the mean projected response of the CORDEX-AFRICA ensemble to external radiative forcing for the considered emissions scenario; (2) the total associated uncertainty; (3) the relative contribution of the different uncertainty components; and (4) the individual contribution of each model to model uncertainty. The main steps of QUALYPSO are as follows (additional details on the method can be found in Evin et al. 2019):

1. For each of the 14 GCM/RCM combinations (Table 1), we extract the precipitation forced response by fitting a trend model (cubic smoothing spline).
2. For each of the 14 GCM/RCM combinations, we compute the relative difference between the trend values estimated for a future period and a reference period respectively (taken here as 1976–2005).

3. Decomposition of the precipitation response using an ANOVA model. Using data augmentation and Bayesian methods, we estimate the ensemble mean (hereafter the ensemble mean precipitation forced response $\mu(t)$), and the deviations of each GCM and each RCM from this ensemble mean precipitation forced response $\mu(t)$.
4. The dispersion (variance) between the main effects obtained for the different GCMs (resp. RCMs) gives an estimate of the model uncertainty due to GCMs (resp. RCMs). We refer to this dispersion as GCM (resp. RCM) uncertainty in the text.
5. Internal unforced variability is estimated as the variance of the deviations from the precipitation forced responses of each of the 14 GCM/RCM combinations. Hence, internal variability in our study refers to the variability of 20-year running mean deviations from the precipitation forced response, and thereby excludes interannual variability.
6. We compute the variance of total uncertainty T(t) as follows:

$$\mathrm{T}(t) = \mathrm{IV}(t) + \mathrm{G}(t) + \mathrm{R}(t) + \mathrm{RES}(t) \tag{1}$$

where T(t), IV(t), G(t), R(t), and RES(t) correspond to the variance of total uncertainty, internal variability, GCM uncertainty, RCM uncertainty, and residual variability (part of the dispersion in the forced precipitation responses that cannot be explained by the ANOVA model, i.e., by the sum of the main effects obtained for the different GCMs and the RCMs), respectively.

We compute the standard deviation of total uncertainty STD(t) (hereafter the standard deviation of the ensemble STD(t)), as follows:

$$\mathrm{STD}(t) = (\mathrm{T}(t))^{\delta}, \tag{2}$$

2.3 Evaluation of the robustness of the projected changes

QUALYPSO estimates are produced for each time step. In Fig. 1, we present results obtained for precipitation changes between 2080–2100 and 1976–2005 (hereafter 2090), expressed in relative terms (% as compared with 1976–2005). Following Christensen et al. (2019), we estimate the robustness of the ensemble mean precipitation forced response $\mu(t)$ by computing the response-to-uncertainty ratio R2U(t), as the ratio between the ensemble mean precipitation forced response $\mu(t)$ and the standard deviation of the ensemble STD(t). Thus, when the absolute value of R2U is >1, the magnitude of the ensemble mean forced response $\mu(t)$ exceeds the standard deviation of the ensemble STD(t), and the response is considered as robust.

In Fig. 2, we present results over the full time period 1976–2100, as averaged over the nine regions depicted in Supplementary Fig. 2, and expressed in relative terms (% as compared with 1976–2005). Shown are the ensemble mean forced precipitation response $\mu(t)$, and the limits of the interval $\mu(t) \pm 1.645$ STD(t), thus representing the 90% uncertainty range. Also shown are the fractions of total uncertainty explained by the different uncertainty components, computed as the ratio between the variance of each uncertainty component, i.e., IV(t), G(t), R(t), and RES(t) and the variance of total uncertainty T(t). Following previous studies (Hawkins and Sutton 2009; Hawkins and Sutton 2011; Hingray and Saïd 2014; Lehner et al. 2020), we compute this 90% uncertainty range additively and symmetrically around the ensemble mean precipitation forced response $\mu(t)$, even though the assumption of

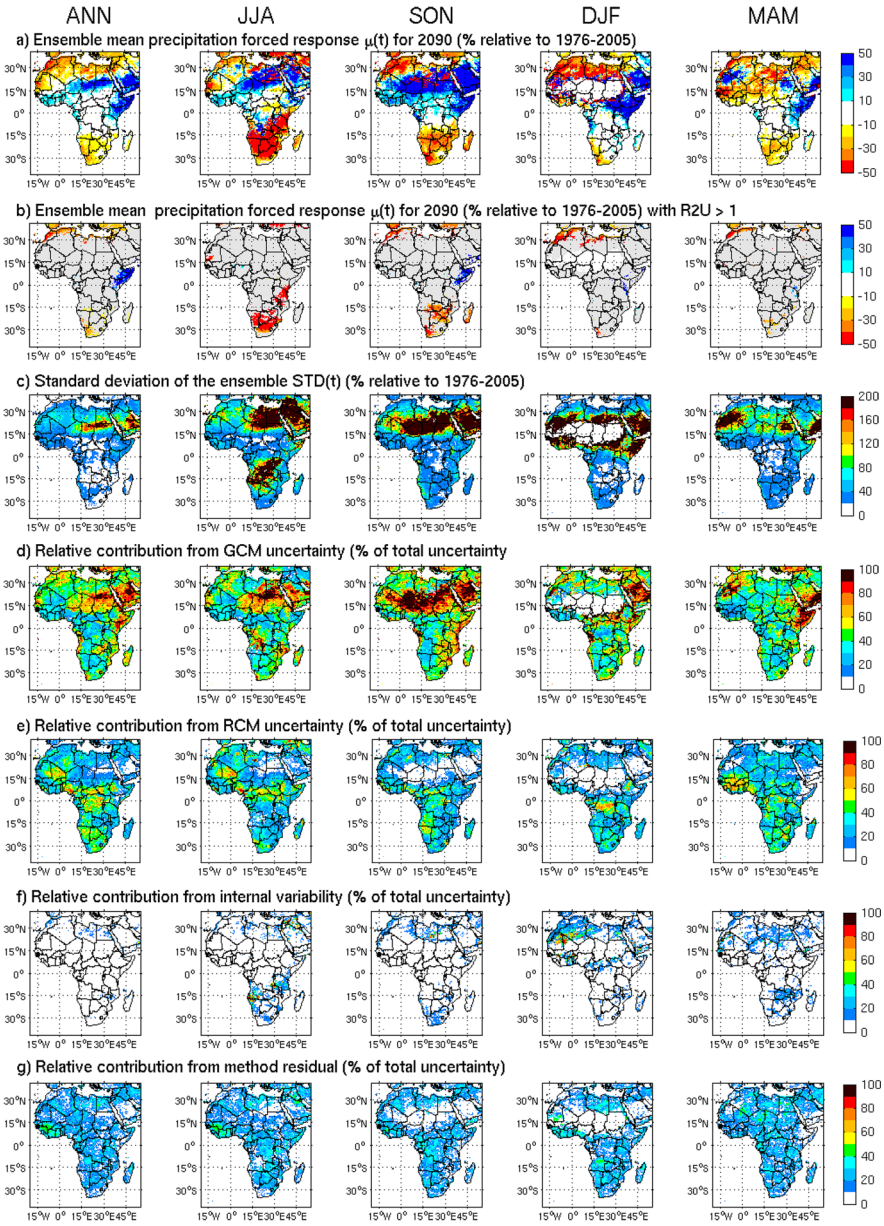

Fig. 1 (**a**) Annual and seasonal ensemble mean precipitation forced response μ(t) for 2090 (% relative to 1976–2005, 20-year running mean). (**b**) as in (**a**) but with the gray shaded areas corresponding to grid points where R2U < 1. Note that there is no data when at least one of the simulation is equal to 0 in the reference period (e.g., over the Sahara in DJF). (**c**) Total uncertainty, shown as the standard deviation of the ensemble STD(*t*) (% relative to 1976–2005), and (**d**–**g**) relative contribution of (**d**) the GCM uncertainty (part of the dispersion in the climate responses of the different GCM/RCM combinations explained in the ANOVA model by the dispersion between the main effects of the different GCMs), (**e**) the RCM uncertainty (part of the dispersion in the climate responses of the different GCM/RCM combinations explained in the ANOVA model by the dispersion between the main effects of the different RCMs), (**f**) internal variability, and (**g**) method residual (part of the dispersion in the climate responses that cannot be explained in the ANOVA model by the sum of the main effects for the GCM and RCM respectively), expressed in % of contribution to the total uncertainty

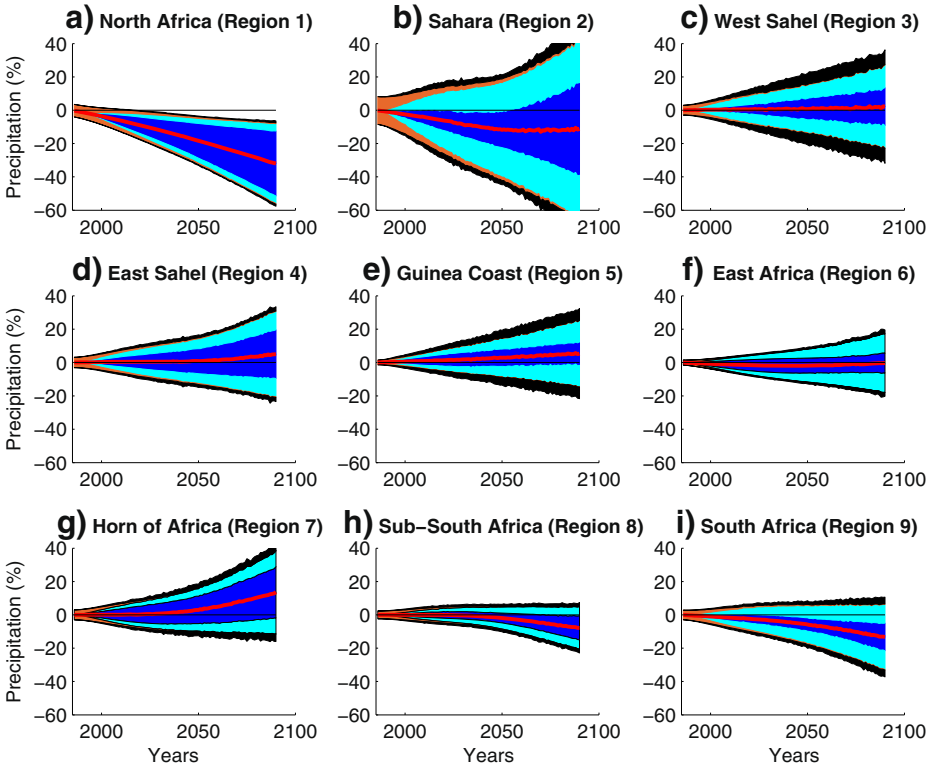

Fig. 2 Ensemble mean precipitation forced response $\mu(t)$ and total uncertainty in 20-year running mean precipitation, as averaged over the nine regions depicted in Supplementary Fig. 2, and expressed in % relative to 1976–2005. The total colored area covered by all uncertainty components corresponds to $\mu(t) \pm 1.645$ STD(t) where STD(t) is the standard deviation of the ensemble (i.e., total uncertainty). The time axis gives the midpoint of the averaging future period. Uncertainty components are shown in dark blue for GCM uncertainty, light blue for RCM uncertainty, orange for internal variability, and black for method residual. For each uncertainty component, the vertical extent of the corresponding area is proportional to the fraction of total uncertainty explained by the component. This fraction is obtained from the ratio between the variance of each uncertainty component (i.e., IV(t), G(t), R(t), and RES(t)) and the variance of total uncertainty T(t)

symmetry is an approximation. Thus, Fig. 2 should only be regarded as an illustration rather than a quantitative depiction of the multi-model uncertainty.

3 Results

3.1 Projected changes in 2090

Figure 1a shows the ensemble mean precipitation forced response $\mu(t)$ of annual, JJA, SON, DJF, and MAM mean precipitation for 2090. By 2090, the annual mean is projected to increase by up to + 50% over the Horn of Africa (excluding the Ethiopian Highlands; + 0.4 mm/day; Supplementary Figs. 4 and 5) and southeastern Sahara (< + 0.2 mm/day), and + 20% along with parts of the Guinea Coast (up to + 0.6 mm/day) and the eastern Sahel (< + 0.2 mm/day). It is projected to decrease on average by − 30% over the western Sahel

(Mauritania, Senegal; < − 0.2 mm/day), the northern coast (from Morocco to Egypt; up to − 0.6 mm/day), northern Sahara (Algeria, Libya, Egypt; < − 0.2 mm/day), and southern Africa (south of 15° S; − 0.4 mm/day). In JJA, the ensemble mean precipitation forced response is projected to increase by up to + 50% over parts of the Horn of Africa (< + 0.2 mm/day) and eastern Sahara (< + 0.2 mm/day), and + 20% along parts of the Guinea Coast (+ 1 mm/day) and eastern Sahel (< + 0.2 mm/day). It is projected to decrease by up to − 50% over the western Sahel (Mauritania, Senegal; up to − 1 mm/day) and southern Africa (south of 15° S plus Tanzania; − 0.4 mm/day), on average by − 30% over the northern coast (from Morocco to Tunisia; − 0.4 mm/day), and on average by − 20% over parts of equatorial Africa (including the Great Lakes area; − 0.6 mm/day). During SON, the ensemble mean precipitation forced response is projected to increase by more than + 50% over the Horn of Africa (+ 0.6 mm/day) and most of the Sahara (< + 0.2 mm/day), and on average by + 30% over the Guinea Coast (+ 1 mm/day) and eastern Sahel (< + 0.2 mm/day). It is projected to decrease on average by − 30% across the northern coast (from Morocco to Tunisia; up to − 0.6 mm/day) and southern Africa (south of 15° S plus Tanzania; up to − 1 mm/day). In DJF, the ensemble mean precipitation forced response is projected to increase by more than + 50% over parts of the Horn of Africa (+ 0.4 mm/day), and decrease on average by − 30% over northern Africa (northern coast (from Morocco to Egypt; up to − 0.6 mm/day) and northern Sahara (Algeria, Libya, Egypt; < − 0.2 mm/day)) and southwestern Africa (from Namibia to South Africa; − 0.4 mm/day). In MAM, the ensemble mean precipitation forced response is projected to increase on average by + 50% over the Horn of Africa (excluding the Ethiopian Highlands; + 0.6 mm/day) and parts of western Sahara (parts of Mauritania and Algeria; < + 0.2 mm/day), and decrease on average by − 30% north of the equator (including the Sahel and Guinea Coast; up to − 0.6 mm/day, and parts of the northern coast of Morocco and the Ethiopian Highlands; − 0.4 mm/day) and south of 15°S (up to − 0.6 mm/day).

Figure 1b is identical to Fig. 1a but the gray shaded area shows regions where the projected changes are not robust, i.e., R2U < 1. According to Fig. 1b, the projected changes considered as robust include the precipitation increase over the Horn of Africa (excluding the Ethiopian Highlands) from September to November and in the annual mean, as well as the precipitation increase over the northern coast (from Morocco to Tunisia) from September to May and in the annual mean, and over southern Africa (south of 15° S) from June to November and in the annual mean.

At this point, it is worth noting that over the dry regions (e.g., Sahara) or during the dry seasons (e.g., Sahel and Guinea Coast in DJF; Horn of Africa in JJA), large changes in relative terms correspond to small changes in absolute values (mm/day; Supplementary Fig. 4) and are not robust. In the next section, we characterize the different sources of uncertainty associated with these projections.

3.2 Partitioning the 2090 uncertainty

Figure 1c illustrates the total uncertainty associated, shown as the standard deviation of the ensemble STD(t). According to Fig. 1c, total uncertainty is particularly large over the Sahara in all seasons, southern Africa in JJA (dry season), Horn of Africa in JJA and DJF, northern coast in JJA, and Guinea Coast and Sahel in DJF (dry season). Conversely, it is relatively small over the northern coast in SON, DJF, and MAM; Guinea Coast and Sahel in JJA, SON, and MAM (wet season); Horn of Africa in SON; central Africa in SON and MAM; and southern Africa in SON, DJF, and MAM (wet season).

To illustrate the breakdown of total uncertainty, Fig. 1d–g show the relative contribution, in % of total uncertainty, of GCM uncertainty (Fig. 1d), RCM uncertainty (Fig. 1e), internal variability (Fig. 1f), and method residual (Fig. 1g). According to Fig. 1d, the relative contribution of GCM uncertainty reaches up to 100% in JJA and SON over the Sahara, 60% on average over southern Africa (up to 80% over the eastern part in SON), 80% on average over the Horn of Africa (excluding the Ethiopian Highlands; up to 100% in SON, DJF, and MAM), 70% on average over the northern coast (up to 80% in MAM), 60% (80%) on average in MAM (JJA and SON) over the eastern Sahel, 60% on average over the western Sahel, and 50% on average over the Guinea Coast (30% in MAM). According to Fig. 1e, the relative contribution of RCM uncertainty to total uncertainty is 40% on average over the southern Africa, 20% on average over the Horn of Africa in JJA (excluding the Ethiopian Highlands), 30% on average over the northern coast (up to 50% in JJA), 40% (20%) on average in MAM (JJA and SON) over the eastern Sahel, 40% on average over the western Sahel, 50% on average over the Guinea Coast (70% in MAM), and 60% over the equatorial Africa (including the Ethiopian Highlands and the Great Lakes area, especially in JJA). In all regions and seasons, the relative contributions from internal variability (excluding interannual variability in this work) and method residual are relatively small ($< 10\%$ and $< 20\%$, respectively).

3.3 Time evolution of the projected changes and associated uncertainties

Supplementary Fig. 6a shows the ensemble mean precipitation forced response $\mu(t)$ of annual, JJA, SON, DJF, and MAM mean precipitation for 2090 (identical to Fig. 1a). Supplementary Fig. 6b and c are identical to Supplementary Fig. 6a but for 2050 and 2030, respectively. According to Supplementary Fig. 6b (6c), the annual and seasonal changes of the ensemble mean precipitation forced response $\mu(t)$ projected for 2050 (2030) are similar to the changes projected for 2090 (Supplementary Fig. 6a), albeit with a smaller amplitude and smaller spatial extent. More specifically, Supplementary Fig. 6 shows that the ensemble mean forced precipitation response annual mean is projected to increase over the Horn of Africa on average by $+20$, $+30$, and $+50\%$ in 2030, 2050, and 2090 respectively, and over the Guinea Coast and the eastern Sahel by $< +10$, $< +10$, and $+20\%$ in 2030, 2050, and 2090 respectively. In contrary, it is projected to decrease over western Sahel on average by -20, -30, and -50% in 2030, 2050, and 2090 respectively, over the northern coast on average by -20, -30, and -40% in 2030, 2050, and 2090 respectively, and over southern Africa on average by < -10, -20, and -30% in 2030, 2050, and 2090 respectively. Additional analyses (Supplementary Figs. 7 and 8) show that the spatial pattern of the different uncertainty components is also similar in 2030, 2050, and 2090.

To illustrate how the relative contribution of the different uncertainty components evolves through time and depends on the region, Fig. 2 shows the 20-year running mean ensemble mean precipitation forced response $\mu(t)$ over 1976–2100 (red curve), as averaged over the nine regions depicted in Supplementary Fig. 2, and expressed in % relative to 1976–2005. Also shown are the 90% uncertainty range of the ensemble, and the relative contribution of each uncertainty component (different color shades). According to Fig. 2, total uncertainty increases over time in all regions, and the relative contribution of internal variability falls below 10% after about 10 years of simulation (i.e., 2015), in favor of model uncertainty. Over time, GCM uncertainty dominates over North Africa, East Sahel, and the Horn of Africa, whereas GCM uncertainty equals RCM uncertainty over the

Sahara, West Sahel, Sub-South Africa and South Africa, and RCM uncertainty dominates over Guinea Coast and East Africa.

4 Discussion

In this study, we use an advanced Bayesian method to estimate the mean projected precipitation "forced response", i.e., the mean projected response of the CORDEX-AFRICA ensemble to external radiative forcing for the considered emissions scenario, over Africa for the twenty-first century, and characterize the different sources of associated uncertainty. We find that the spatial pattern of the projected changes is identical throughout the twenty-first century and that its amplitude increases with time. In this section, we discuss the results for each region separately.

4.1 Eastern Africa

Over the Horn of Africa (excluding the Ethiopian Highlands), we find that the ensemble mean precipitation forced response is projected to increase over the twenty-first century (on average by + 20, + 30, and + 50% by 2030, 2050, and 2090, respectively; Supplementary Fig. 6) in SON (+ 0.6 mm/day by 2090), DJF (+ 0.4 mm/day by 2090), and MAM (+ 0.6 mm/day by 2090). However, this increase is robust only in SON due to a strong GCM uncertainty (> 80%) in all seasons that results mostly from GCMs CSIRO (DJF), IPSL (MAM), and MIROC (JJA and SON; Supplementary Fig. 9).

Our projections are coherent with those obtained by Niang et al. (2014) expecting more intense wet seasons (MAM and JJA) and less severe droughts in MAM and SON, suggesting an increase in the likelihood of floods and a decrease in the likelihood of droughts. In this dry region (annual mean below 2 mm/day; Supplementary Fig. 1), decreasing the likelihood of droughts would be beneficial for society, which already suffers regularly from extreme droughts.

In addition, the dryer conditions projected over the northern part of the Great Lakes in JJA (Fig. 1a) and the Ethiopian Highlands in MAM (Supplementary Fig. 4) are also in agreement with previous studies (Niang et al. 2014; Dosio et al. 2019) and are expected to occur mostly under the form of less frequent (and less intense in the case of the Ethiopian Highlands) rainfall (Niang et al. 2014; Dosio et al. 2019). However, this drying is not robust due to a strong RCM uncertainty that results mostly from RCM CLMcom (Supplementary Fig. 10).

At this point, it is worth noting that over the past 30 years, the observations (e.g., Cattani et al. 2018) show a partial decrease (recovery) of precipitation in MAM (SON) over parts of eastern Africa, including the Ethiopian Highlands (Horn of Africa). As our projections (i.e., precipitation response to external radiative forcing) show a decrease (increase) of precipitation over the Ethiopian Highlands in MAM (Horn of Africa in SON), we suggest that these recent trends result from external radiative forcing. It is important to recall however that the mechanisms driving the recent (after 1980) precipitation trends in this region are still poorly understood, potentially involving complex connections with the Indian Ocean (e.g., Williams et al. 2012), the Atlantic Ocean (Seleshi and Zanke 2004), and the Pacific Ocean (e.g., Philip et al. 2018). This could be why the poor performance of individual CORDEX RCMs in East Africa was shown in a number of studies such as Ayugi et al. (2020), Onyutha (2020), Endris et al. (2013), and Kisembe et al. (2018).

4.2 Northern coast and southern Africa

Over the northern coast (from Morocco to Tunisia) and the southern part of Africa (south of 15° S), the ensemble mean precipitation forced response is projected to decrease (on average by − 20, − 30, and − 40% by 2030, 2050, and 2090, respectively over the northern coast, and by < − 10, − 20, and − 30% by 2030, 2050, and 2090, respectively, over southern Africa; Supplementary Fig. 6) all year long. Over the northern coast of Africa, this decrease (up to − 0.6 mm/day by 2090 in SON, DJF, and MAM, and − 0.4 mm/day by 2090 in JJA) is robust only over the coast of Morocco from September to May. Elsewhere over the region, the results are not robust due to a strong GCM uncertainty (70%) in all seasons that results mostly from GCMs CSIRO (DJF and MAM), IPSL (SON), and IPSL and MIROC (JJA; Supplementary Fig. 9). Over southern Africa, this decrease (− 1 mm/day by 2090 in SON, − 0.6 mm/day by 2090 in MAM, and − 0.4 mm/day by 2090 in DJF and JJA) is robust only over localized parts of the region from June to November. Elsewhere over the region, the results are not robust due to a strong uncertainty from GCMs (60%) and RCMs (40%) in all seasons. The GCM uncertainty results mostly from GCMs CSIRO and MIROC (DJF and MAM), CCCma and CSIRO (SON), and ICHEC (JJA; Supplementary Fig. 9), and the RCM uncertainty results mostly from RCMs SMHI (DJF and JJA), KNMI (MAM), and SMHI and DMI (SON; Supplementary Fig. 10).

In these dry regions (annual mean below 2 mm/day; Supplementary Fig. 1), such a drying trend would be damageable for society.

4.3 Sahel

Over western Sahel, we find that the ensemble mean precipitation forced response is projected to decrease (on average by − 20, − 30, and − 50% by 2030, 2050, and 2090, respectively; Supplementary Fig. 6) at the beginning (< 0.2 mm/day by 2090 in MAM) and during (− 1 mm/day by 2090 in JJA) the rainy season. However, this decrease is not robust due to a strong uncertainty from GCMs (about 60%) and RCMs (about 40%) in all seasons. The GCM uncertainty results mostly from GCMs MIROC (MAM), CSIRO and CNRM (SON), and CCCma and MIROC (JJA; Supplementary Fig. 9), and the RCM uncertainty results mostly from RCMs CLMcom (MAM), DMI, CLMcom, and KNMI (SON), and SMHI and CLMcom (JJA; Supplementary Fig. 10).

Our projections are in good agreement with annual (− 0.5 mm/day by 2100; Todzo et al. 2020) and seasonal (− 30% by 2090 in May–September; Sylla et al. 2016) downscaled projections. According to the authors, the projected drying is expected to occur as more intense (+ 1.35 mm/day by 2100 in Todzo et al. 2020; + 30% in May–September by 2090 in Sylla et al. 2016) but less frequent (− 27 wet days in a year by 2100 in Todzo et al. 2020; + 60% maximum dry spell length in May–September by 2090 in Sylla et al. 2016) precipitation, which is expected to increase the drought conditions and the likelihood for floods in this already vulnerable region. In this dry region (annual mean below 2 mm/day; Supplementary Fig. 1), such a drying would be damageable for society, which is already regularly suffering from severe droughts.

Over eastern Sahel, we find that the ensemble mean precipitation forced response is projected to decrease (on average by < − 10, − 20 and − 30% by 2030, 2050, and 2090, respectively; Supplementary Fig. 6) at the beginning of the rainy season (< − 0.2 mm/day by 2090 in MAM), and increase (on average by < + 10, + 15, and + 25% by 2030, 2050, and

2090, respectively) during and at the end of the rainy season (< + 0.2 mm/day by 2090 in JJA and SON). However, in MAM, these projections are not robust due to a strong uncertainty from GCMs (about 60%) and RCMs (about 40%) in all seasons. The GCM uncertainty results mostly from GCMs IPSL and MIROC (Supplementary Fig. 9) while the RCM uncertainty results mostly from RCM CLMcom (Supplementary Fig. 10). In JJA and SON, these projections are not robust due to a strong GCM uncertainty (> 80%) in all seasons that result mostly from GCMs CCCma and CSIRO (SON), and CCCma and MIROC (JJA; Supplementary Fig. 9).

Our projections are in good agreement with seasonal downscaled projections (+ 15% in May–September by 2090; Sylla et al. 2016). According to the authors, precipitation is projected to intensify by the end of the twenty-first century (+ 2 mm/day by 2100 in Todzo et al. 2020; + 20% in May–September by 2090 in Sylla et al. 2016), which is expected to increase the likelihood for floods in this region. In this dry region (annual mean below 2 mm/day; Supplementary Fig. 1), the projected increase (decrease) during and at the end of the rainy season (at the beginning of the rainy season) would be beneficial (damageable) for society, which already suffers regularly from severe droughts.

At this point, it is worth noting that over the past 30 years, the observations (e.g., Panthou et al. 2014; Bichet and Diedhiou 2018a) showed a clear increase in the Sahelian (eastern and western) precipitation during the rainy season (June to September). In our projections however (i.e., precipitation response to external radiative forcing), mean precipitation is projected to decrease over western Sahel throughout the rainy season (March to November), and decrease (increase) over eastern Sahel in MAM (JJA and SON). Hence, we suggest that the recent increase observed over the Sahel mostly results from internal variability over western Sahel, and from external radiative forcing over eastern Sahel. It is important to remind that up to this date, mechanisms leading to this so called recent "Sahel rainfall recovery" is still under debate, as it can be both attributed to natural variability (Mohino et al. 2011) or a forced response to increased greenhouse gases (Haarsma et al. 2005; Biasutti 2013) or reduced aerosols (Ackerley et al. 2011).

4.4 Guinea Coast

Over the Guinea Coast, the ensemble mean precipitation forced response is projected to decrease (on average by < − 10%, − 20 and − 30% by 2030, 2050, and 2090, respectively; Supplementary Fig. 6) during the first rainy season (− 0.6 mm/day by 2090 in MAM), and increase (on average by < + 10, + 20, and + 25% by 2030, 2050, and 2090, respectively; Supplementary Fig. 6) during the little dry season and the second rainy season (+ 1 mm/day by 2090 in JJA and SON). However, in MAM, these projections are not robust due to a strong RCM uncertainty (about 70%) in all seasons that results mostly from RCM CLMcom (Supplementary Fig. 10). In JJA and SON, these projections are not robust due to a strong uncertainty from GCMs (50%) and RCMs (50%) in all seasons. The GCM uncertainty results mostly from GCMs CSIRO (SON) and MIROC (JJA; Supplementary Fig. 9) whereas the RCM uncertainty results mostly from RCM DMI (Supplementary Fig. 10).

Our projections are in good agreement with annual (+ 0.8 mm/day by 2100; Todzo et al. 2020) and seasonal (+ 15% in May–September by 2090; Sylla et al. 2016) downscaled projections. According to the authors, precipitation is projected to intensify (+ 2.7 mm/day by 2100 in Todzo et al. 2020; + 20% in May–September by 2090 in Sylla et al. 2016) and rarefy (− 13.5 wet days in a year by 2100 in Todzo et al. 2020; + 60% maximum dry spell

length in May–September by 2090 in Sylla et al. 2016), which is expected to increase the likelihood of floods and droughts. Whereas this humid region (annual mean on average 4 mm/day; Supplementary Fig. 1) is not particularly threatened by droughts, it regularly suffers from severe floods, and increasing the intensity of floods further would be disastrous for society.

At this point, it is worth noting that over the past 30 years, the observations (Bichet and Diedhiou 2018b) show a clear increase in precipitation over the Guinea Coast during the second rainy season (SON). Since this is also the case in our projections (precipitation response to external radiative forcing only), we suggest that the recent increase observed over the Guinea Coast in SON results from external radiative forcing.

5 Conclusion

In agreement with previous global and regional climate projections (e.g., Niang et al. 2014; Sylla et al. 2016; Todzo et al. 2020), we find that in the twenty-first century, mean precipitation is projected to increase over the Horn of Africa from September to May and over the Guinea Coast in JJA, SON, and the annual means, but decrease over the Ethiopian Highlands in MAM, the northern part of the Great Lakes area in JJA, the northern coast (from Morocco to Tunisia) and southern Africa (south of 15° S) all year long, and the Sahel in JJA and annual means. In addition, we also find that it is projected to increase over eastern Sahel and the Guinea Coast in JJA and SON, decrease over western Sahel in MAM and JJA, and decrease in the Sahel and the Guinea Coast in MAM. These changes are projected to become more pronounced throughout the twenty-first century.

In agreement with Hawkins and Sutton (2009 and 2011), our results show that total uncertainty increases with time and that the contribution from internal variability falls very rapidly compared to model uncertainty. This leads to the fact that over most regions, the changes projected for 2090 are not robust, i.e., smaller than the associated uncertainty. According to our results, GCMs, namely MIROC, CSIRO, and to a lesser extent CCCma and IPSL strongly contribute to this uncertainty over the Horn of Africa (80%), northern coast (70%), and eastern Sahel (80% in JJA and SON). Both GCM and RCM equally contribute to this uncertainty over the Sahara, Guinea Coast (JJA and SON), eastern Sahel (MAM), western Sahel and southern Africa (60%), and RCMs, namely CLMcom and to a lesser extent DMI and SMHI) strongly contribute to this uncertainty over the Guinea Coast (70% in MAM) and parts of Eastern Africa such as the Great Lakes and the Ethiopian Highlands (60% in JJA). Hence, even though downscaled projections from CORDEX-AFRICA add value to global climate projections (e.g., over western Africa and parts of eastern Africa), our results show that over highly convective regions such as the Guinea Coast, Great Lakes, and Ethiopian Highlands, regional climate projections suffer from large uncertainties that result mostly from the RCMs. This suggests, in agreement with Klutse et al. (2015) and Koné et al. (2018), that the different parametrization schemes for convection may play an important role explaining the disagreements across the models of CORDEX-AFRICA. In particular, we suggest that the Mesoscale Convective Systems (MCSs), known to produce 50–90% of the rainfall over equatorial Africa including the Sahel (e.g., Jackson et al. 2009; Taylor et al. 2017; Nicholson 2018), are poorly represented in CORDEX-AFRICA RCMs because they occur on scales that are not resolved by these models. Additional work using RCMs explicitly resolving convection would be required to fully address this issue. Over the Horn of Africa, northern coast, and eastern Sahel however, regional climate projections suffer from large uncertainties

that result mostly from the GCMs, introduced through their large-scale meteorological fields used as boundary conditions of RCMs (air temperature, humidity, zonal and meridional wind, geopotential height, surface air pressure, and sea surface temperatures). Because some individual models contribute to model (GCMs and RCMs) uncertainty more strongly than others (e.g., the GCMs MIROC, CSIRO, CCCma, and IPSL and the RCM CLMcom), our study also raises the question of understanding the different factors of divergence.

The large uncertainties found in our work imply that over most regions (except for North Africa), even the sign of change is uncertain, and even though the projected mean change is relatively small, important changes may actually occur in reality. In addition, although we find a relatively small contribution of internal variability (falls below 10% after about 10 years of simulation in all regions), it is important to keep in mind that in our study, internal variability (1) does not include interannual variability, which in reality will modulate significantly the forced response and will lead to large year-to-year variations at all scales (e.g., seasonal, annual; Sun et al. 2018), (2) corresponds to internal variability simulated by the CORDEX-AFRICA models, which has not been evaluated against observed internal variability, (3) is assumed to be constant through time (limitation of the QUALYPSO method), and (4) is estimated from single-run ensembles, i.e., when only one experiment is available for each GCM/RCM combinations (limitation of the CORDEX-AFRICA database), which raises the need for modeling centers to release more multi-run ensembles in the future, as it would allow a more accurate estimation of natural variability and a solid evaluation of natural variability against observations, as well as a more accurate estimation of the precipitation forced response for each GCM/RCM combination (Hingray et al. 2019).

Additional limitations of our study include (1) the limitations inherent to the CORDEX-AFRICA dataset, including the poor representation of some sub-scale processes such as the MCSs and the poor representation of the impacts of atmospheric aerosols, particularly abundant over West Africa due to seasonal desert dusts but only partially accounted for in CORDEX-AFRICA (Liousse et al. 2014; Ghan and Penner 2016; N'Datchoh et al. 2018), and (2) additional sources of uncertainty not accounted for in QUALYPSO, including the quality of the projection, which varies greatly from a region to another (Supplementary Figs. 1 and 3). Note also that to reliably assess long-term rainfall changes, it is vital to characterize natural variation in terms of the statistical dependence (Onyutha et al. 2019). However, our study did not consider long-range dependence but focused on the various sources of uncertainty based on Bayesian ANOVA. Nevertheless, our work allows a first estimation of the importance of this natural variability in regional climate projections, and we suggest that in order to be useful for decision-makers, similar studies should be carried out at the local level. At last, even though the identification of the driving mechanisms behind these projections is beyond the scope of this study, the results suggest that the external forcing has an impact in the Guinea Coast and eastern Sahel through similar mechanisms, though the mechanisms involved in MAM are different from those involved in JJA and SON. In addition, they suggest that the western Sahel responds to a different mechanism than its eastern counterpart during and at the end of the rainy season (in JJA and SON, respectively) and that unlike the rest of West Africa, western Sahel seems particularly influenced by internal variability.

Acknowledgments The authors acknowledge the usage of the CHIRPS data set from the Climate Hazards Group (http://chg.geog.ucsb.edu/data/chirps) and the usage of the CORDEX-AFRICA data set from the World Climate Research Program's Working Group on Regional Climate (http://www.cordex.org/data-access/esgf/).

Contribution of the authors The authors declare to have no conflict of interest with this work. A. Bichet, A. Diedhiou, and B. Hingray fixed the analysis framework. G. Evin produced the estimates of the different sources of uncertainty using QUALYPSO. A. Bichet carried out all other calculations and analyses and produced graphs. All authors contributed to the redaction.

Funding The research leading to this publication is co-funded by the NERC/DFID "Future Climate for Africa" program under the AMMA-2050 project, grant number NE/M019969/1, by IRD (Institut de Recherche pour le Développement; France) grant number UMR IGE Imputation 252RA5" and by the French National program LEFE (Les Enveloppes Fluides et l'Environnement).

Compliance with ethical standards

Conflict of interest The authors declare that they have no conflict of interest.

References

Ackerley D, Booth BBB, Knight SHE, Highwood EJ, Frame DJ, Allen MR, Rowell DP (2011) Sensitivity of twentieth-century Sahel rainfall to sulfate aerosol and CO2 forcing. J Clim 24:499–5014. https://doi.org/10.1175/JCLI-D-11-00019.1

Anyamba A, Small JL, Britch SC, Tucker CJ, Pak EW, Reynolds CA et al (2014) Recent weather extremes and impacts on agricultural production and vector-borne disease outbreak patterns. PLoS One 9(3):e92538. https://doi.org/10.1371/journal.pone.0092538

Ayugi B, Tan G, Gnitou GT, Ojara M, Ongoma V (2020) Historical evaluations and simulations of precipitation over East Africa from Rossby centre regional climate model. Atmos Res 232:104705

Biasutti M (2013) Forced Sahel rainfall trends in the CMIP5 archive. J Geophys Res-Atmos 118:1613–1623. https://doi.org/10.1002/jgrd.50206

Bichet A, Diedhiou A (2018a) West African Sahel has become wetter during the last 30 years, but dry spells are shorter and more frequent. Clim Res 75:155–162

Bichet A, Diedhiou A (2018b) Less frequent and more intense rainfall along the coast of the Gulf of Guinea in West and Central Africa (1981−2014). Clim Res 76:191–201

Bichet A, Hingray B, Evin G, Diedhiou A (2019) Potential impact of climate change on solar resource in Africa: analyses from CORDEX-AFRICA experiments. Environ Res Lett 14:124039. https://doi.org/10.1088/1748-9326/ab500a

Boko M, Niang I, Nyong A, Vogel C, Githeko A, Medany M, Osman-Elasha B, Tabo R, Yanda P (2007) Africa climate change 2007: impacts, adaptation and vulnerability. In: Parry ML, Canziani OF, Palutikof JP, van der Linden PJ, Hanson CE (eds) Contribution of working group II to the fourth assessment report of the intergovernmental panel on climate change. Cambridge University Press, Cambridge, pp 433–467

Cattani E, Merino A, Guijarro JA, Levizzani A (2018) East Africa rainfall trends and variability 1983-2015 using three long-term satellite products. Remote Sens 10(6):1–26. https://doi.org/10.3390/rs10060931

Christensen JH, Hewitson B, Busuioc A, Chen A, Gao X, Held I, Jones R, Kolli RK, Kwon WT, Laprise R, Magaña Rueda V, Mearns L, Menéndez CG, Räisänen J, Rinke A, Sarr A, Whetton P (2007) Regional climate projections. In: Solomon S, Qin D, Manning M, Chen Z, Marquis M, Averyt KB, Tignor M, Miller HL (eds) Climate change 2007: the physical science basis. Contribution of Working Group I to the Fourth Assessment Report of the Intergovernmental Panel on Climate Change. Cambridge University Press, Cambridge

Christensen JH, Krishna Kumar K, Aldrian E, An SI, Cavalcanti IFA, de Castro M, Dong W, Goswami P, Hall A, Kanyanga JK, Kitoh A, Kossin J, Lau NC, Renwick J, Stephenson DB, Xie SP, Zhou T (2013) Climate phenomena and their relevance for future regional climate change. In: Stocker TF, Qin D, Plattner GK, Tignor M, Allen SK, Boschung J, Nauels A, Xia Y, Bex V, Midgley PM (eds) Climate change 2013: the physical science basis. Contribution of Working Group I to the Fifth Assessment Report of the Intergovernmental Panel on Climate Change. Cambridge University Press, Cambridge

Christensen JH, Larsen MAD, Christensen OB, Drews M, Stendel (2019) Robustness of European climate projections from dynamical downscaling. Clim Dyn 53:4857–4869

Dai A (2013) Increasing drought under global warming in observations and models. Nat Clim Chang 3:52–58. https://doi.org/10.1038/nclimate1633

Diedhiou A, Bichet A, Wartenburger R, Seneviratne SI, Rowell DP, Sylla MB et al (2018) Changes in climate extremes over West and Central Africa at 1.5 C and 2 C global warming. Environ Res Lett 13(6):065020

Donat MG, Pitman AJ, Angélil O (2018) Understanding and reducing future uncertainty in midlatitude daily heat extremes via land surface feedback constraints. Geophys Res Lett 45(19):10–627

Dosio A, Jones RG, Jack C, Lennard C, Nikulins G, Hewitson B (2019) What can we know about future precipitation in Africa? Robustness, significance and added value of projections from a large ensemble of regional climate models. Clim Dyn 53:5833–5858. https://doi.org/10.1007/s00382019-04900-3

Douglas I, Alam K, Maghenda M, McDonnell Y, Mclean L, Campbell J (2008) Unjust waters: climate change, flooding and the urban poor in Africa. Environ Urban 20:187–205. https://doi.org/10.1177/0956247808089156

Endris HS, Omondi P, Jain S, Lennard C, Hewitson B, Chang'a L, Awange JL, Dosio A, Ketiem P, Nikulin G, Panitz HJ, Büchner M, Stordal F, Tazalika L (2013) Assessment of the performance of CORDEX regional climate models in simulating East Africa rainfall. J Clim 26:8453–8475

Evin G, Hingray B, Blanchet J, Eckert N, Morin S, Verfaillie D (2019) Partitioning uncertainty components of an incomplete ensemble of climate projections using data augmentation. J Clim 32:2423–2440. https://doi.org/10.1175/JCLI-D-18-0606.1

Fontaine B, Roucou P, Gaetani M, Marteau R (2011) Recent changes in precipitation, ITCZ convection and northern tropical circulation over North Africa (1979–2007). Int J Climatol 31(5):633–648

Funk C, Peterson P, Landsfeld M, Pedreros D et al (2015) The climate hazards infrared precipitation with stations — a new environmental record for monitoring extremes. Scientific Data 2:150066

Ghan S, Penner JE (2016) ARM-led improvements in aerosols in climate and climate models. Meteorol Monogr 27(5):1–12

Giorgi F, Coppola E, Raffaele F (2014) A consistent picture of the hydroclimatic response to global warming from multiple indices: models and observations. J Geophys Res-Atmos 119. https://doi.org/10.1002/2014JD022238

Giorgi F, Francisco R (2000) Uncertainties in regional climate change prediction: a regional analysis of ensemble simulations with the HADCM2 coupled AOGCM. Clim Dyn 16:169–182

Giorgi F, Jones C, Asrar G (2009) Addressing climate information needs at the regional level. The CORDEX framework. WMO Bull 58:175–183

Haarsma RJ, Selten FM, Weber SL, Kliphuis M (2005) Sahel rainfall variability and response to greenhouse warming. Geophys Res Lett 32:L17702. https://doi.org/10.1029/2005GL023232

Hawkins E, Sutton R (2009) The potential to narrow uncertainty in regional climate predictions. Bull Am Meteorol Soc 90:1095–1107. https://doi.org/10.1175/2009BAMS2607.1

Hawkins E, Sutton R (2011) The potential to narrow uncertainty in projections of regional precipitation change. Clim Dyn 37(1–2):407–418

He JJ, Yu Y, Yu LJ, Liu N, Zhao SP (2017) Impacts of uncertainty in land surface information on simulated surface temperature and precipitation over China. Int J Climatol 37:829–847

Hewitson B, Lennard C, Nikulin G, Jones C (2012) CORDEX-Africa: a unique opportunity for science and capacity building. CLIVAR Exchanges 17(3):6–7

Hingray B, Blanchet J, Evin G, Vidal JP (2019) Uncertainty components estimates in transient climate projections. Precision of estimators in the single time and time series approaches. Clim Dyn 53:2501–2516. https://doi.org/10.1007/s00382-019-04635-1

Hingray B, Saïd M (2014) Partitioning internal variability and model uncertainty components in a multimember multimodel ensemble of climate projections. J Clim 27:6779–6798. https://doi.org/10.1175/JCLI-D-13-00629.1

Jackson B, Nicholson SE, Klotter D (2009) Mesoscale convective systems over western equatorial Africa and their relationship to large-scale circulation. Mon Weather Rev 137:1272–1294. https://doi.org/10.1175/2008MWR2525.1

Jones CG, Giorgi F, Asrar G (2011) The coordinated regional downscaling experiment: CORDEX; an international downscaling link to CMIP5. CLIVAR Exchanges. International CLIVAR Project Office, 56, Southampton, 34-40

Kisembe J, Favre A, Dosio A, Lennard L, Sabiiti G, Nimusiima A (2018) Evaluation of rainfall simulations over Uganda in CORDEX regional climate models. Theor Appl Climatol 137(1–2):1117–1134

Klutse NAB, Sylla MB, Diallo I, Sarr A, Dosio A, Diedhiou A, Kamga A, Lamptey B, Ali A, Gbobaniyi EO, Owusu K, Lennard C, Hewitson B, Nikulin G, Panitz HJ, Büchner M (2015) Daily characteristics of West African monsoon rainfall in CORDEX regional climate models. Theor Appl Climatol 123:369–386. https://doi.org/10.1007/s00704-014-1352-3

Koster RD, Dirmeyer PA, Guo Z, Bonan G, Chan E, Cox P et al (2004) Regions of strong coupling between soil moisture and precipitation. Science 305(5687):1138–1140

Koné B, Diedhiou A, N'Datchoh ET, Sylla MB, Giorgi F, Anquetin S et al (2018) Sensitivity study of the regional climate model RegCM4 to different convective schemes over West Africa. Earth Syst Dyn 9(4): 1261–1278

Lehner F, Deser C, Maher N, Marotzke J, Fischer E, Brunner L, Knutti R, Hawkins E (2020) Partitioning climate projection uncertainty with multiple large ensembles and CMIP5/6. Earth System Dynamics Discussions, 1–28. https://doi.org/10.5194/esd-2019-93

Liousse C, Assamoi E, Criqui P, Granier C, Rosset R (2014) Explosive growth in African combustion emissions from 2005 to 2030. Environ Res Lett 9:035003

Lobell DB, Schlenker WS, Costa-Roberts J (2011) Climate trends and global crop production since 1980. Science 333:616–620. https://doi.org/10.1126/science.1204531

Mohino E, Janicot S, Bader J (2011) Sahel rainfall and decadal to multi-decadal sea surface temperature variability. Clim Dyn 37(3):419–440. https://doi.org/10.1007/s00382-010-0867-2

N'Datchoh ET, Diallo I, Konaré A, Silué S, Ogunjobi KO, Diedhiou A, Doumbia M (2018) Dust induced changes on the West African summer monsoon features. Int J Climatol 38:452–466. https://doi.org/10.1002/joc.5187

Nicholson SE (2018) The ITCZ and the seasonal cycle over equatorial Africa. Bull Am Meteorol Soc 99:337–348. https://doi.org/10.1175/BAMS-D-16-0287.1

Niang I, Ruppel OC, Abdrabo MA, Essel A, Lennard C, Padgham J, Urquhart P (2014) Africa. In: Climate change 2014: impacts, adaptation, and vulnerability. Part B: regional aspects. Contribution of Working Group II to the Fifth Assessment Report of the Intergovernmental Panel on Climate Change [Barros VR, Field CB, Dokken DJ, Mastrandrea MD, Mach KJ, Bilir TE, Chatterjee M, Ebi KL, Estrada YO, Genova RC, Girma B, Kissel ES, Levy AN, MacCracken S, Mastrandrea PR, White LL (eds.)]. Cambridge University Press, Cambridge, pp. 1199–1265

Nikulin G, Jones C, Giorgi F, Asrar G, Büchner M, Cerezo-Mota R, Christensen OB, Déqué M, Fernandez J, Hänsler A, van Meijgaard E, Samuelsson P, Sylla MB, Sushama L (2012) Precipitation climatology in an ensemble of CORDEX-Africa regional climate simulations. J Clim 25:6057–6078

Onyutha C, Rutkowska A, Nyeko-Ogiramoi P, Willems P (2019) How well do climate models reproduce variability in observed rainfall? A case study of the Lake Victoria basin considering CMIP3, CMIP5 and CORDEX simulations. Stoch Env Res Risk A 33:687–707. https://doi.org/10.1007/s00477-018-1611-4

Onyutha C (2020) Analyses of rainfall extremes in East Africa based on observations from rain gauges and climate change simulations by CORDEX RCMs. Clim Dyn 54:4841–4864

Orlowsky B, Seneviratne S (2012) Global changes in extreme events: regional and seasonal dimension. Clim Chang 110:669–696

Panthou G, Vischel T, Lebel T (2014) Recent trends in the regime of extreme rainfall in the Central Sahel. Int J Climatol 34:3998–4006

Philip S, Kew SF, van Oldenborgh GJ, Otto F, O'Keefe S, Haustein K et al (2018) Attribution analysis of the Ethiopian drought of 2015. J Clim 31(6):2465–2486. https://doi.org/10.1175/JCLI-D-17-0274.1

Roehrig R, Bouniol D, Guichard F, Hourdin F, Redelsperger JL (2013) The present and future of the west African monsoon: a process-oriented assessment of CMIP5 simulations along the AMMA transect. J Clim 26:6471–6505. https://doi.org/10.1175/JCLI-D-12-00505.1

Rowell D (2012) Sources of uncertainty in future changes in local precipitation. Clim Dyn 39:1929–1950

Schewe J, Heinke J, Gerten D, Haddeland I, Arnell NW, Clark DB et al (2014) Multi-model assessment of water scarcity under climate change. PNAS 111(9):3245–3250. https://doi.org/10.1073/pnas.1222460110

Seleshi Y, Zanke U (2004) Recent changes in rainfall and rainy days in Ethiopia. Int J Climatol 24(8):973–983

Seneviratne SI, Nicholls N, Easterling D, Goodess CM, Kanae S, Kossin J, Luo Y, Marengo J, McInnes K, Rahimi M, Reichstein M, Sorteberg A, Vera C, Zhang X (2012) Changes in climate extremes and their impacts on the natural physical environment. In: Managing the risks of extreme events and disasters to advance climate change adaptation [Field CB, Barros V, Stocker TF, Qin D, Dokken DJ, Ebi KL, Mastrandrea MD, Mach KJ, Plattner GK, Allen SK, Tignor M, Midgley PM (eds.)]. A special report of

Working Groups I and II of the Intergovernmental Panel on Climate Change (IPCC). Cambridge University Press, Cambridge, pp. 109–230
Sun F, Roderick ML, Farquhar GD (2018) Rainfall statistics, stationarity, and climate change. Proc Natl Acad Sci U S A 115(10):2305–2310
Sylla MB, Nikiema PM, Gibba P, Kebe I, Klutse NAB (2016) Climate change over West Africa: recent trends and future projections. In: Yaro JA, Hesselberg J (eds) Adaptation to climate change and variability in rural West Africa. Springer International Publishing, Basel, pp 25–40
Taylor CM, Beluši D, Guichard F, Parker DJ et al (2017) Frequency of extreme Sahelian storms tripled since 1982 in satellite observations. Nature 544:475–478
Todzo S, Bichet A, Diedhiou A (2020) Intensification of the hydrological cycle expected in West Africa over the 21st century. Earth Syst Dyn 11:319–328. https://doi.org/10.5194/esd-11-319-2020
Williams AP, Funk C, Michaelsen J, Rauscher SA, Robertson I, Wils THG, Koprowski M, Eshetu Z, Loader NJ (2012) Recent summer precipitation trends in the greater horn of Africa and the emerging role of Indian Ocean sea surface temperature. Clim Dyn 39(9–10):2307–2328. https://doi.org/10.1007/s00382-011-1222-y
Zwiers FW, Alexander LV, Hegerl GC, Knutson TR, Kossin J, Naveau P, Nicholls N, Schär C, Seneviratne SI, Zhang X (2013) Challenges in estimating and understanding recent changes in the frequency and intensity of extreme climate and weather events. In: Asrar GR, Hurrell JW (eds) Climate science for serving society: research, modeling and prediction priorities. https://doi.org/10.1007/978-94-007-6692-1_13

Affiliations

Adeline Bichet[1] · Arona Diedhiou[1,2] · Benoit Hingray[1] · Guillaume Evin[3] · N'Datchoh Evelyne Touré[2] · Klutse Nana Ama Browne[4] · Kouakou Kouadio[2]

[1] University Grenoble Alpes, IGE UMR 5001, 38400 Saint Martin d'Hères, France

[2] African Center of Excellence on Climate Change, Biodiversity and Sustainable Agriculture (LAPAMF, CEA-CCBAD), University Félix Houphouët Boigny, Abidjan, Côte d'Ivoire

[3] INRAE, ETNA, Saint Martin dHères, France

[4] University of Ghana, Legon, Greater Accra, Ghana